

Effect of Solidification Rate and Composition on Microstructure and Crystallization in Al-Ni-La Metallic Glasses

K.L. Sahoo¹, M. Wollgarten² and J. Banhart²

¹National Metallurgical Laboratory, Jamshedpur-831007, India.

²Department of Materials, Hahn-Meitner-Institut Berlin, 14109, Berlin, Germany.

E-mail: klsah@nmlindia.org

(Received 30 June 2006 ; in revised form 20 November 2006)

ABSTRACT

Al₈₇La₇Ni_{6-x}Ag_x (x = 0,1) alloys, prepared by copper mould casting and melt-spinning at different wheel speeds, were studied by X-ray diffraction, scanning electron microscopy, differential scanning calorimetry and microhardness measurements. The Cu-mould cast ingot shows a hypereutectic microstructure. At the highest cooling rate (wheel speed 40 m/s) the ribbon is completely amorphous, while at lower wheel speeds mixed structures comprising amorphous and crystalline phases or only crystalline phases were observed. Both the ribbons (with and without Ag containing alloys) show two-stage crystallization process on annealing. Crystallization kinetics was analysed by Kissinger and Johnson-Mehl-Avrami approaches. The low values of activation energy reflect the instability of these amorphous alloys. Microhardness of all the ribbons was examined at different temperatures and was correlated with the corresponding evolution of phases.

1. INTRODUCTION

Al-based amorphous alloys, in particular those containing transition metal (TM) and rare earth (RE) elements, are promising candidates as structural materials for industrial applications because of their favourable combination of physical and mechanical properties^{1,2}. Mechanical properties can be further improved by ensuring a uniform distribution of fcc-Al nanoparticles in the amorphous matrix by appropriate heat treatment³. The initial microstructure of the alloy influences the kinetics of the phase transformation upon heating. The rate of solidification during liquid state to solid state plays an important role in determining the initial state of the as-cast structures. At low solidification rate (normal sand cast or chill cast condition) the competition between eutectic and independent growth of phases is a crucial factor that determines the solidification microstructure of the alloys. At higher cooling rates the formation of equilibrium phases is suppressed. When a liquid is cooled to below the liquidus temperature, crystallization does not begin everywhere at once. A certain amount of time is required for the formation and growth of crystals. If the liquid is cooled very rapidly from above the liquidus temperature to below the glass temperature so that there is no time for crystals to form, an amorphous structure is created if the alloy system obeys some basic requirements of metallic glass formation. Crystallization changes the properties of amorphous alloys. Growth of crystallites can be retarded by choice of the alloy

composition that leads to higher activation energy of crystallization. Among the Al-based metallic glass systems, Al-Ni-La is especially promising because of the wide glass formation range and good glass forming ability. The formation of primary crystallites and their crystallization kinetics have been studied by a number of research groups for several Al-based amorphous alloys⁴⁻⁶. Gangopadhyay and Kelton⁷ investigated the crystallization process in Al-Ni-RE amorphous alloys and found that crystallization products depend upon the radius of the rare earth atoms. They showed that alloys containing RE elements with smaller atomic radii form fcc-Al while RE elements with larger atomic radii first transform into metastable intermetallic phases and then subsequently to stable phases upon heating. The formation of initial microstructure on solidification rate and the primary crystallization products upon annealing as-cast ribbons in Al-Ni-La systems depends on the amount of La added. The reports on the addition of another transition metal by partial replacement of Ni are meagre and it may change in the initial microstructure and alterations in crystallization kinetics. The effect of solidification rate and the effect of partial substitution of Ni by another transition metal (Ag) on the initial microstructure and crystallization kinetics were discussed in this paper.

2. EXPERIMENTAL

Ingots of composition Al₈₇Ni₆La₇ and Al₈₇Ni₅Ag₁La₇ were prepared by alloying the pure elements (purity of Al: 5N; Ni: 4N; La: 3N; Ag: 4N) by induction-levitation melting under a purified argon atmosphere and by casting and quenching the melt in a water cooled copper mould of 3 mm diameter (cooling rate ~ 10² K/s). The microstructure of the ingot was examined by scanning electron microscopy (SEM) and phases were identified by X-ray diffractometry (XRD). Each ingot was inductively re-melted and melt-spun ribbons were prepared in an argon atmosphere. The speed of the rotating wheel varied to vary the cooling rate and to obtain ribbons with different thicknesses. The thickness of the ribbons and the initial microstructure were determined. The crystallization behaviour of the ribbons was studied by differential scanning calorimetry (DSC). Isochronal DSC studies were conducted at different heating rates ranging from 10 to 40 K/min. For scanning at a constant heating rate a second scan on the same sample was used as a base line. For isothermal DSC analysis the as-melt-spun ribbons were heated to minimum three desired temperatures for each crystallization stage at a rate of 100 K/min and held up to 20 minutes before rapid

cooling to room temperature. The evolution of hardness with temperature was investigated using a microhardness tester applying a load of 0.2 N.

3. RESULTS AND DISCUSSION

3.1 Mould cast alloys

In both cast rods ($\text{Al}_{87}\text{Ni}_6\text{La}_7$ and $\text{Al}_{87}\text{Ni}_5\text{La}_7\text{Ag}_1$) the major phases present are identified as α -Al, $\text{Al}_{11}\text{La}_3$, Al_3La and Al_3Ni (Fig. 1). These binary phases are in accordance with the equilibrium phase diagram in Al-La-Ni system⁸. Some of the diffraction peaks of very low intensity could not be identified and presumable belong to ternary phases of Al, La and Ni (marked as 'o' in Fig. 1). Literature also reports some of the ternary intermetallic phases e.g., Al_3LaNi_2 , Al_5LaNi_2 in Al-Ni-La system⁹. A representative SEM micrograph of $\text{Al}_{87}\text{Ni}_6\text{La}_7$ ingot is shown in Fig. 2. SEM studies revealed that the primary $\text{Al}_{11}\text{La}_3$ and Al_3Ni phases are uniformly distributed in the matrix of α -Al. EDS analysis of the eutectic composition revealed the binary eutectic composition of Al/ $\text{Al}_{11}\text{La}_3$ and Al/ Al_3Ni instead of ternary Al- $\text{Al}_{11}\text{La}_3$ - Al_3Ni eutectic which is generally obtained in fully eutectic microstructure in alloy composition $\text{Al}_{94.7}\text{Ni}_{2.8}\text{La}_{2.5}$ ¹⁰. The formation of binary eutectics in hypereutectic alloys may be explained such that after the formation of primary phases of $\text{Al}_{11}\text{La}_3$, Al_3Ni and α -Al one of the binary eutectic components nucleates prior to the other one. The Al- Al_3Ni eutectic would probably nucleate first because its eutectic temperature (640°C) appears to be higher than that for the Al- $\text{Al}_{11}\text{La}_3$ eutectic¹⁰. Trapping of some of the Al_3Ni phase in a primary $\text{Al}_{11}\text{La}_3$ phase (Fig. 2) indicates that the Al_3Ni dendrites had a higher growth temperature under the present conditions than the $\text{Al}_{11}\text{La}_3$ phases. No appreciable difference in equilibrium phase formation was found in the alloy containing 1 at% Ag.

3.2 Melt-spun alloys

The melt spun ribbons were prepared by ejecting the melt on the rotating Cu-Be wheel (single roller). The width and thickness of the ribbons depend on the wheel speed, crucible orifice diameter, height of the orifice to the wheel etc. The

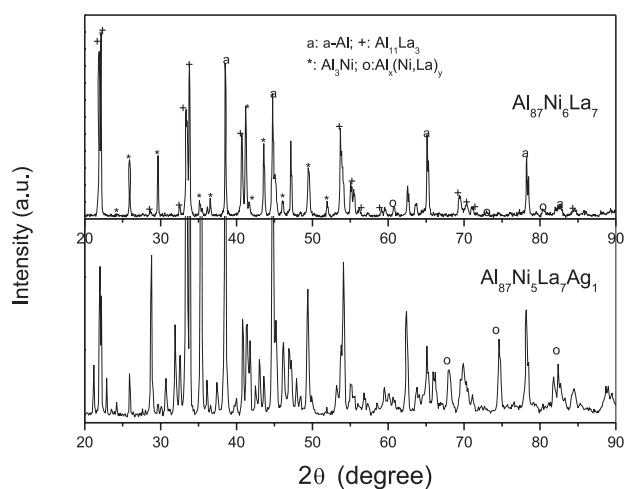


Fig. 1 : XRD pattern of crystalline $\text{Al}_{87}\text{Ni}_6\text{La}_7$ and $\text{Al}_{87}\text{Ni}_5\text{La}_7\text{Ag}_1$ ingots. Phases are marked with symbols.

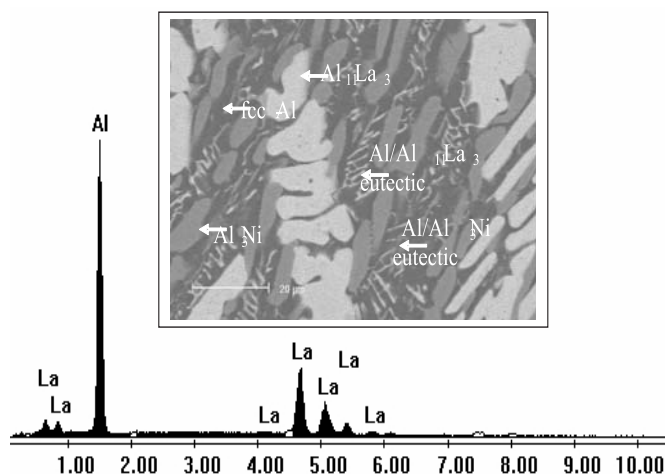


Fig. 2 : SEM back-scattered image of $\text{Al}_{87}\text{Ni}_6\text{La}_7$ ingot, phases are marked. EDS signal showing Al + La only in primary $\text{Al}_{11}\text{La}_3$ phase.

rate of cooling depends thickness of ribbon, heat transfer coefficient, surface quality of the wheel, wetting, heat capacity of the melt etc. However, in general, the cooling rate achieved in a single roller melt spinning system is 10^5 to 10^6 K/s. As the measurement of cooling rate is not possible in the present melt spinning system, we report the change of cooling rate by changing the rotational speed of the wheel. On changing the cooling rate by changing the wheel speed the thickness of the ribbons and their microstructure changes. Table 1 summarises the alloy condition, thickness of the ribbon and structure of the as-quenched state. All the melt-spun $\text{Al}_{87}\text{Ni}_6\text{La}_7$ ribbons up to the thickness of 60 μm show good bending ductility. XRD studies revealed that these ribbons were fully amorphous on the substrate side (not shown) as well as on the air-cooled side (Fig. 3). In case of $\text{Al}_{87}\text{Ni}_5\text{La}_7\text{Ag}_1$ alloy at a maximum wheel speed (40 m/s) the ribbons are completely amorphous. The wheel speed mentioned in the text is the linear speed which is

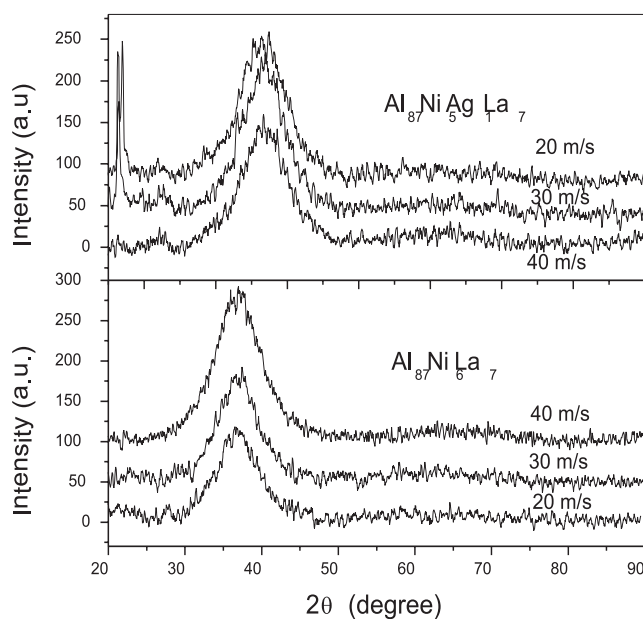


Fig. 3 : XRD patterns of as-melt-spun amorphous ribbons on the air-cooled side at wheel speeds of 20, 30 and 40 m/s.

Table 1

Alloy composition and wheel speed on the thickness and structure of ribbons.

| alloy | wheel speed, m/s | thickness, mm | structure of the as-quenched state |
|--|------------------|---------------|------------------------------------|
| Al ₈₇ Ni ₆ La ₇ | 40 | 30±2 | amorphous |
| Al ₈₇ Ni ₆ La ₇ | 30 | 37±2 | amorphous |
| Al ₈₇ Ni ₆ La ₇ | 20 | 60±5 | amorphous |
| Al ₈₇ Ni ₅ Ag ₁ La ₇ | 40 | 33±2 | amorphous |
| Al ₈₇ Ni ₅ Ag ₁ La ₇ | 30 | 37±2 | amorphous + crystalline |
| Al ₈₇ Ni ₅ Ag ₁ La ₇ | 20 | 60±2 | amorphous + crystalline |
| Al ₈₇ Ni ₅ Ag ₁ La ₇ | 10 | 90±2 | crystalline |
| Al ₈₇ Ni ₅ Ag ₁ La ₇ | 5 | 215±10 | crystalline |

circumference of the wheel (in m) times the rotational speed (in revolution per second). At lower wheel speeds (30 and 20 m/s) the ribbons comprise a mixed structure of mostly amorphous regions and small fraction of crystalline phases. But at these wheel speeds (30 and 20 m/s) the base alloy shows the completely amorphous on substrate as well as on air-cooled side. This clearly indicates that the partial replacement of Ni by Ag deteriorates the ability of the melt to form glasses. This may be due to wide equilibrium solid solubility of Ag in Al (23.8 at.%). At 10 and 5 m/s wheel speeds Ag containing ribbons are mostly crystalline and hence, not further discussed. The amorphous as-melt-spun ribbons showed a distinct broad diffuse maximum centred on 37°, which is a characteristic of a glassy phase.

The ribbons are heated continuously in a DSC at various heating rates. Fig. 4 shows representative DSC curves of the amorphous alloys heated at a rate of 40 K/min. The number of heat events as well as their position on the temperature axis change with alloy composition. Two exothermic peaks corresponding to the crystallization of phases are observed in different temperature ranges. Definite differences between the two systems in both the peak temperature of the first

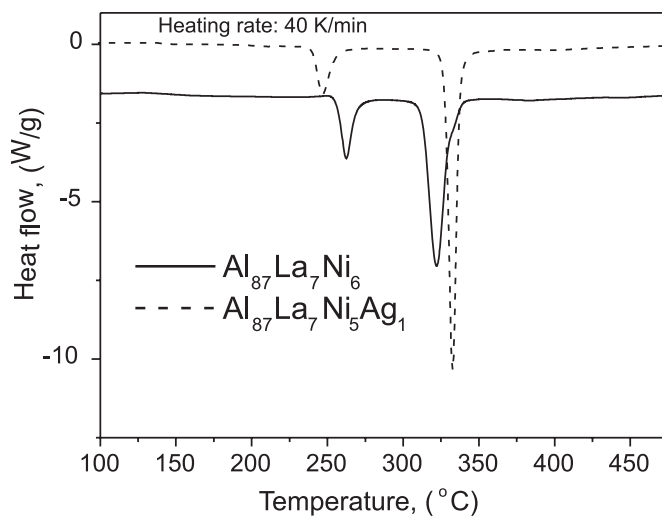


Fig. 4 : Continuous heating DSC curves of as-melt-spun amorphous ribbons at a heating rate of 40 K/min.

crystallization (T_{x1p}) as well as the second crystallization (T_{x2p}) stages were observed. T_{x1p} of the Al₈₇Ni₆La₇ ribbon is larger than that of the Ag containing ribbon, while T_{x2p} of the Ag-containing ribbon is larger than that of Al₈₇Ni₆La₇. The peak temperatures of crystallization increases with increasing heating rate which can be used to obtain an estimate for the activation energies (E_a) of crystallization using Kissinger analysis ¹¹;

$$\ln\left(\frac{T_p^2}{\beta}\right) = \left(\frac{E_a}{RT_p}\right) + A$$

where β is the heating rate, T_p is the peak temperature in Kelvin, R is the gas constant, and A is a fitting constant. The activation energy is calculated from the slope of the linear

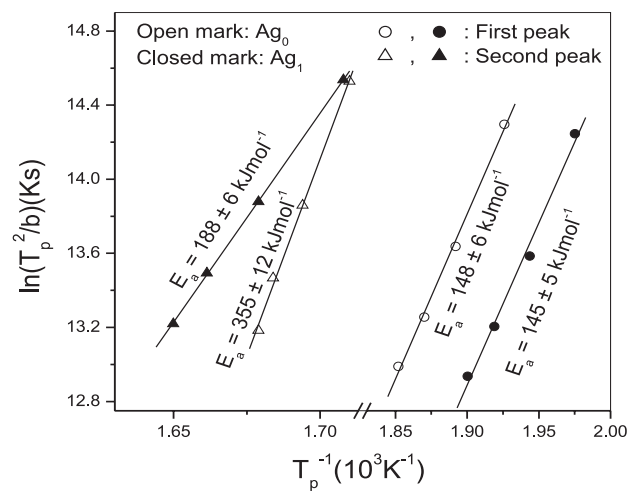


Fig. 5a : The Kissinger plot of peak temperatures of first and second stage reactions, open mark base alloy and closed mark Ag containing alloy. Wheel speed 40 m/s.

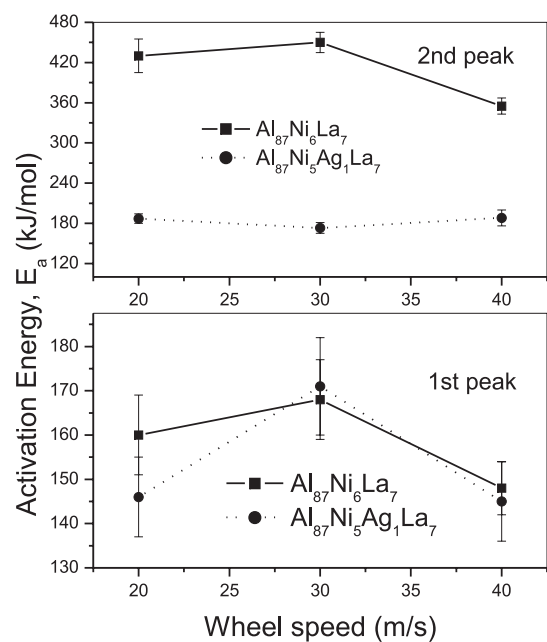


Fig. 5b : Variation of activation energies with wheel speed for first and second crystallization stages.

plot of $\ln(T_p^2/\beta)$ as a function of peak temperature (Fig. 5(a)). The values of activation energies for all crystallization stages in both the alloys at different cooling rate are shown in Fig. 5(b). The low value of activation energy during the first stage of crystallization reflects the high instability of these glasses. Obviously, the activation energy of the second stage of crystallization for the Ag-containing ribbon is much less than that for the Ag-free ribbon. The first peak for the Ag-containing ribbon moves to lower temperature, and the second peak moves to higher temperature compared to Ag-free ribbon indicate that the replacement of Ni by Ag causes the increase in the precipitation tendency of nanoscale metastable particles and the retardation of the decomposition of the remaining amorphous phase. Literature¹² also reports the addition of Ag on Al-Ni-Ce alloys refines the precipitation of fcc-Al and decreases its activation energy. Small angle neutron scattering experiment (unpublished results) indicated that Ag-containing glass contains small clusters/concentration fluctuations which is much higher in number but smaller in size than the Ag-free glass. The presence of these clusters helps in occurrence of early crystallization stages. After the first stage of crystallization the remaining matrix is richer in alloying elements and thus retards its decomposition. Ag was added in order to obtain a wider difference between primary and secondary crystallization temperature. This is helpful while producing the alloy, containing nanocrystals in fcc-Al matrix, in bulk through ribbon/powder – compaction – extrusion route.

In order to identify the different phases responsible for the two crystallization stages observed in the DSC curve, different samples were heated in the DSC up to the end of the individual heat events, after which the same samples were analysed by XRD. The first stage i.e., the primary crystallization stage in both the alloys is due to the formation of a metastable phase (Fig. 6) that transforms to a stable fcc Al-phase (Fig. 6) at higher temperatures. After primary crystallization the structure contains a uniform distribution of metastable phase in an amorphous matrix. The second crystallization stage is due to the formation of stable intermetallic compounds ($\text{Al}_{11}\text{La}_3$, Al_3La , Al_3Ni) and fcc Al-phase from the amorphous matrix and the transformation of metastable phase to stable phase (Fig. 6).

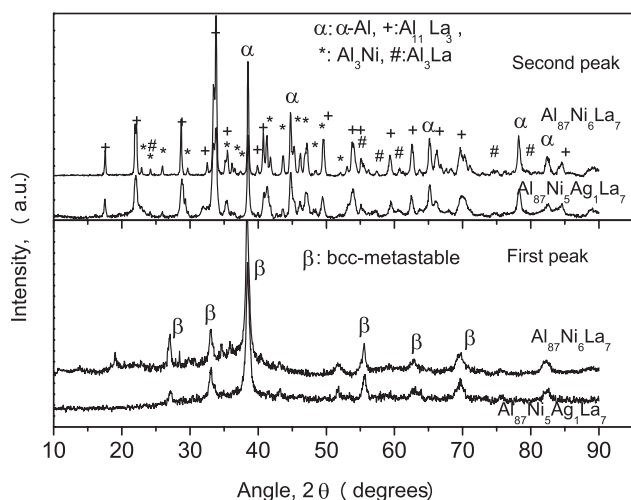


Fig. 6 : XRD patterns of $\text{Al}_{87}\text{Ni}_6\text{La}_7$ and $\text{Al}_{87}\text{Ni}_5\text{Ag}_1\text{La}_7$ ribbons after first and second stages of crystallizations.

The crystallization behaviour of these phases during different stages of crystallization was investigated through isothermal DSC studies. Different samples were annealed at different temperatures around the onset temperature of the crystallization stages (isothermal curves are not shown). The isothermal phase transformation is generally described by the well-known Johnson-Mehl-Avrami (JMA) equation for transformation kinetics¹³⁻¹⁴:

$$x = 1 - \exp[-\{K(t-t_0)\}^n],$$

where x denotes the transformed volume fraction at time t , n is JMA exponent, which depends on nucleation rate and growth kinetics, K is the reaction rate constant and t_0 is the time delay. The values of K and n can be determined from the exothermic heat release peaks using the relationship

$$\ln\{\ln[1/(1-x)]\} = n\ln(K) + n\ln(t-t_0)$$

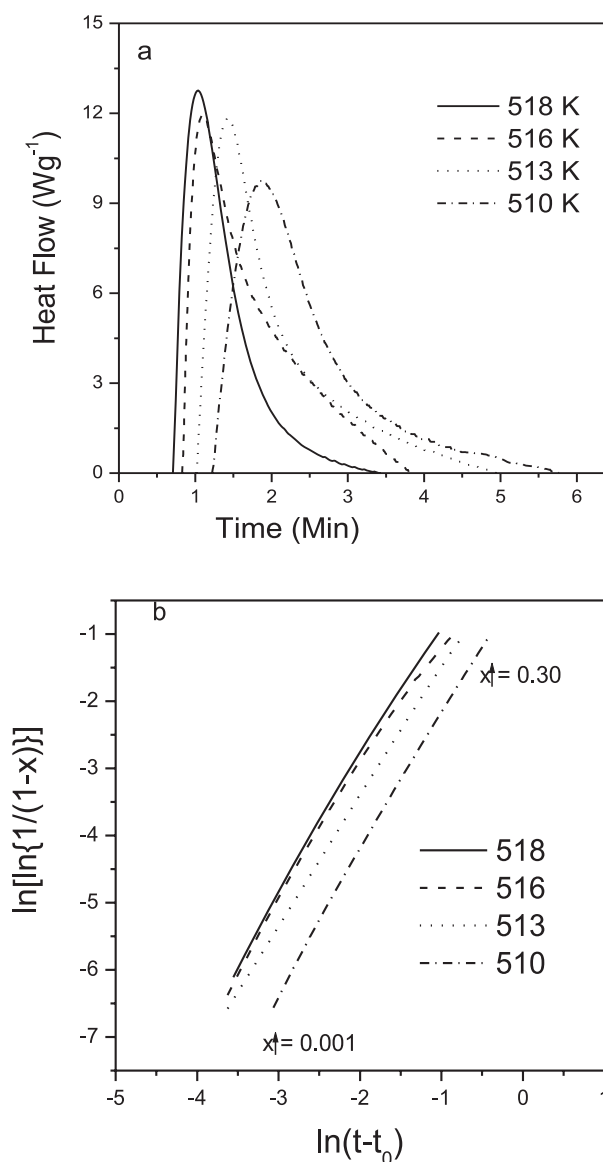


Fig. 7 : (a) Isothermal DSC curves for the first crystallization stage and (b) JMA plots for amorphous $\text{Al}_{87}\text{Ni}_6\text{La}_7$ ribbons annealed at temperatures from 510 to 518 K.

Plots of $\ln\{\ln[1/(1-x)]\}$ against $\ln(t-t_0)$ for each annealing temperature for the first peak of base alloy are shown in Fig. 7. For the range of data approximately between $x = 0$ to 0.35 the graphs (Fig. 7) could be fitted by straight lines. The Avrami exponents, n , for the first peak determined from the slope of the straight part of the line in Fig. 7 and the reaction rate constants K determined by the use of equation are listed in Table 2. The temperature dependence of the reaction rate factor K follows an Arrhenius law with the activation energy for the process, E_c :

$$k = k_0 \exp\left(-\frac{E_c}{RT}\right)$$

where K_0 is a constant. The value of activation energy calculated from the above equation is shown in Table 2. The value of activation energy are in consistent with the values obtained from Kissinger plot.

For the $Al_{87}Ni_6La_7$ ribbon, the average Avrami exponent for the first stage of crystallization is 1.95 ± 0.02 which according to Christian's¹⁵ classification can be interpreted that the precipitates grow from nuclei which are already present in the as-melt-spun ribbons. The n value for the second stage of crystallization of $Al_{87}Ni_6La_7$ ribbon is 2.1 ± 0.06 . Similarly, for $Al_{87}Ni_5La_7Ag_1$ ribbon the average value of n for first and second crystallization stages are 1.9 ± 0.02 and 3.6 ± 0.02 , respectively. Different values of for the Avrami exponent can be an indication for different types of nucleation and growth mechanism, e.g., $n = 1.5$ is indicative of three-dimensional growth with zero nucleation rate, $n = 1.5$ to 2.5 refers to growth with decreasing nucleation rate, $n = 2.5$ advocates for constant nucleation rate and $n > 2.5$ postulates three-dimensional growth with increasing nucleation rate¹⁵. The value of Avrami exponent (1.9 to 2.1) during the first stage of crystallization for both the alloys indicates that the ribbons might contain some quenched-in-nuclei that grow upon heating. Initially, some of these quenched-in-nuclei grow to a certain critical radius to become a nucleus and then growth takes place. Thus, when the amorphous matrix crystallizes during the first crystallization stage the initial nucleation rate is high and thereafter it decreases with time.

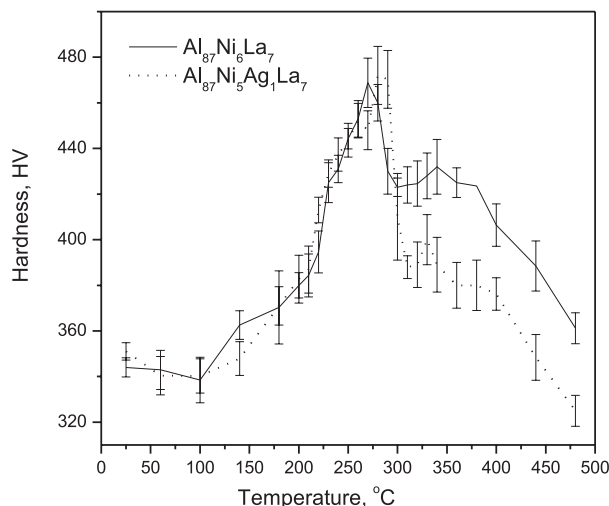


Fig. 8 : Microhardness evolution during isochronal heating of $Al_{87}Ni_6La_7$ and $Al_{87}Ni_5Ag_1La_7$ ribbons. Samples were annealed for 10 minutes at each measuring temperature. Each hardness value is the average of 10 measurements at 0.2 N load. The corresponding statistical error is shown at each data point.

Fig. 8 shows the variation of microhardness with temperature. Individual ribbons were annealed for 10 minutes ranging from room temperature to 480°C. The heating rate up to the annealing temperature was 100 K/min. The hardness values shown in Fig. 8 are the average of about 10 measurements on each sample and the corresponding errors are shown for each data point. During annealing hardness does not change much from room temperature to about 100°C. This is due to fact that the microstructure does not change appreciably as these glasses are thermally stable at lower temperatures. Thereafter, a sharp increase of hardness with increasing temperature is observed which is caused by crystallization of a metastable bcc phase leading to precipitation strengthening of the material. The highest hardness values were detected at around 270°C for $Al_{87}Ni_6La_7$ and at around 280°C for alloy $Al_{87}Ni_5Ag_1La_7$. At the point where the highest hardness is observed the matrix is still amorphous. Crystallization at even higher temperatures (above 280°C for $Al_{87}Ni_5Ag_1La_7$) results

Table 2

Kinetic parameters analysed from the isothermal analysis of the first and second peak crystallization of the amorphous $Al_{87}Ni_6La_7$ (wheel speed 40 m/s).

| Temperature, (K) | t_0 (min) | t_p (min) | Avrami exponent, n | Reaction rate constant, K (min^{-1}) | Activation (E_c) from plot of $\ln K$ vs $1/T$ |
|------------------|-------------|-------------|--------------------|--|--|
| 510 | 1.22 | 1.86 | 2.10 ± 0.01 | 0.95 ± 0.005 | $170 \pm 5 \text{ kJmol}^{-1}$ |
| 513 | 1.02 | 1.42 | 1.91 ± 0.01 | 1.25 ± 0.009 | |
| 516 | 0.83 | 1.08 | 1.95 ± 0.01 | 1.55 ± 0.01 | |
| 518 | 0.71 | 1.02 | 1.97 ± 0.02 | 1.76 ± 0.02 | |
| 565 | 3.38 | 5.14 | 2.03 ± 0.003 | 0.41 ± 0.02 | $389 \pm 26 \text{ kJmol}^{-1}$ |
| 568 | 2.25 | 3.49 | 2.08 ± 0.002 | 0.62 ± 0.01 | |
| 570 | 1.76 | 2.65 | 2.02 ± 0.003 | 0.81 ± 0.01 | |
| 573 | 1.39 | 1.96 | 2.05 ± 0.006 | 1.27 ± 0.02 | |

in a sharp drop of hardness owing to the transformation of metastable to stable phases and the decomposition of the amorphous matrix leading to the precipitation of intermetallic particles (mainly, fcc-Al, $\text{Al}_{11}\text{La}_3$ and Al_3Ni) from the matrix. With progressing crystallization, hardness increases again due to the increased volume fraction of crystallized intermetallic particles. In later stage the observed decrease in hardness with higher temperature can be associated with coarsening of these particles.

4. CONCLUSIONS

$\text{Al}_{87}\text{Ni}_6\text{La}_7$ and $\text{Al}_{87}\text{Ni}_5\text{La}_7\text{Ag}_1$ alloys cast at low cooling rates showed hypereutectic microstructures comprising primary α -Al, $\text{Al}_{11}\text{La}_3$, Al_3Ni phases and Al/ $\text{Al}_{11}\text{La}_3$ and Al/ Al_3Ni eutectics. The structure of the alloy changes when it is cast by melt spinning. The resulting amorphous ribbons undergo a two-stage crystallization process upon heating. The two stages of crystallization correspond to the formation of a metastable bcc-phase and the decomposition of both the amorphous matrix and the metastable phase. The first crystallization temperature decreases while the second one increases with Ag addition.

Hardness does not change appreciably up to 100°C , indicating the structural stability at lower temperatures. Thereafter, the sharp increase in hardness is due to nanoscale precipitation of bcc-metastable phase. The rapid reduction of hardness in $\text{Al}_{87}\text{Ni}_6\text{La}_7$ ribbon after 270°C and in

$\text{Al}_{87}\text{Ni}_5\text{La}_7\text{Ag}_1$ ribbon after 280°C is due to the decomposition of amorphous matrix and metastable phase.

REFERENCES

1. Inoue A, Zhang T, Kita K and Masumoto T, *Mater. Trans. JIM.*, **30** (1989) 870.
2. He Y, Poon S J and Shiflet G, *Science*, **241** (1988) 1640.
3. Inoue A, *Prog. Mater. Sci.*, **43** (1998) 365.
4. Ye F and Lu K, *J. Non-Crys. Solids*, **262** (2000) 228.
5. Allen D R, Foley J C and Perepezko J H, *Acta Metall.*, **46** (1998) 431.
6. Sahoo K L, Rao V and Mitra A, *Mater. Trans.*, **44** (2003) 1075.
7. Gangopadhyay A K and Kelton K F, *Phil. Mag.*, **80A** (2000) 1193.
8. Godecke T, Sun W, Luck R and Lu K, *Z. Metallkd.*, **92** (2001) 7.
9. Cordier G, Dorsam G and Kniep R, *J. Magnetism Magnetic Mater.*, **76** (1988) 653.
10. Hawksworth A, Rainforth W M and Jones H, *Mater. Sci. Eng. A*, **262** (1999) 159.
11. Kissinger H E, *Anal. Chem.*, **29** (1957) 1702.
12. Inoue A, Nakazato K, Kawamura Y and Tsai A P, *Mater. Trans., JIM*, **35** (1994) 95.
13. Johnson W A and Mahl R F, *Trans. Am. Inst. Min. Metall. Eng.*, **135** (1939) 416.
14. Avrami M, *J. Chem. Phys.* **9** (1941) 177.
15. Christian J, *The theory of transformation in metals and alloys. Part 1, Equilibrium and general kinetic theory*, (Pergamon press, Oxford, 1975) 542.